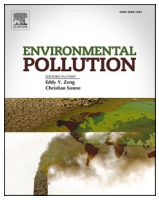
Environmental Pollution 402 (2026) 128408



Contents lists available at ScienceDirect

Environmental Pollution

journal homepage: www.elsevier.com/locate/envpol



Contrasting impacts of policy interventions and population mobility on organic aerosols and oxygenated volatile organic compounds in Beijing

Yu Zhang [a,b,c], Weiqi Xu [a,*], Wei Zhou [a], Jintai Lin [d], Mengying Wang [d], Yan Li [a], Siqi Zeng [a,b], Ziyi Zhang [b,e], Xiaomin Cheng [a,b], Yang Yang [c,f], Yele Sun [a,b]

[a] State Key Laboratory of Atmospheric Environment and Extreme Meteorology, Institute of Atmospheric Physics, Chinese Academy of Sciences, Beijing, 100029, China
[b] College of Earth and Planetary Sciences, University of Chinese Academy of Sciences, Beijing, 100049, China
[c] Hebei Provincial Weather Modification Center, Shijiazhuang, 050021, China
[d] Laboratory for Climate and Ocean–Atmosphere Studies, Department of Atmospheric and Oceanic Sciences, School of Physics, Peking University, Beijing, 100871, China
[e] State Key Laboratory of Earth System Numerical Modeling and Application, Institute of Atmospheric Physics, Chinese Academy of Sciences, Beijing, 100029, China
[f] Key Laboratory of Meteorology and Ecological Environment of Hebei Province, Shijiazhuang, 050021, China

ARTICLE INFO

Keywords:
Emission control efficiency
Meteorological normalization
Source apportionment
Oxidation flow reactor
Air quality

ABSTRACT

Organic aerosol (OA) is a dominant component of fine particulate matter in megacities, yet disentangling the impacts of emission changes from meteorological variability remains a major challenge for air quality management. This study investigates the responses of OA and its gaseous precursors to short-term emission variations in Beijing across six major events from 2014 to 2022, categorized into three policy interventions (the 2014 APEC Summit, the 2015 Victory Day Parade, and the 2022 Winter Olympic Games) and three population mobility events (Chinese New Year holidays in 2019, 2020, and 2021). Using machine-learning-based meteorological normalization, we found that policy interventions involving coordinated local and regional emission controls effectively reduced secondary OA (SOA) by 46–64%, with emission reductions contributing 63–74% of this decrease. In contrast, local-only emission reductions during population mobility events resulted in negligible OA decreases or even increases, as meteorological conditions played a dominant role in driving pollutant accumulation. High-resolution measurements during the 2022 Winter Olympic Games (WOG) revealed that precursor emission controls not only reduced SOA mass but also significantly suppressed aging processes. Specifically, aging-induced SOA enhancement decreased from 0.5 to 0.6 to 0.1–0.3 μg m^{-3} during the WOG period, while the characteristic aging time was reduced from 2.6 to 5.5 to 1.5–3.9 days. Our findings demonstrate that regional coordinated controls are essential for effectively mitigating secondary pollution, whereas the benefits of short-term local emission changes are frequently offset by unfavorable meteorology.

1. Introduction

Air quality in China has improved significantly over the past decade because of the implementation of the Atmospheric Pollution Prevention and Control Action Plan from 2013 to 2017 and the Three-Year Action Plan from 2018 to 2020 (Geng et al., 2024; Li et al., 2023a). Meanwhile, the chemical composition of particulate matter (PM) and volatile organic compounds (VOCs) exhibited significant changes (Chen et al., 2024a; Zheng et al., 2023a). For instance, the contribution of organic aerosol (OA) to $PM_{2.5}$ gradually decreased in winter due to reduced primary emissions, leading to secondary organic aerosol (SOA) becoming the dominant OA component (Lei et al., 2021a). However, Li et al. (2023a) found that the contribution of OA to $PM_{2.5}$ increased in summer during 2018–2022, suggesting that OA responds differently to emission changes in different seasons. Such different responses to control measures (Kenagy et al., 2024; Li et al., 2023b) lead to uncertainties in the accurate prediction of SOA, thereby affecting assessments of pollution control effectiveness.

Previous studies have investigated the responses of SOA and its precursors to short-term emission controls during policy interventions in Beijing, such as the 2014 Asia-Pacific Economic Cooperation ($APEC_{2014}$) Summit (Sun et al., 2016), the 2015 China Victory Day Parade ($V\text{-}Day_{2015}$) (Li et al., 2016a; Zhao et al., 2017), and the Winter Olympic Games in 2022 (WOG_{2022}) (Liu et al., 2022; Qu et al., 2024). During

* Corresponding author.
E-mail address: xuweiqi@mail.iap.ac.cn (W. Xu).

https://doi.org/10.1016/j.envpol.2026.128408
Received 22 October 2025; Received in revised form 20 May 2026; Accepted 21 May 2026
Available online 22 May 2026
0269-7491/© 2026 Elsevier Ltd. All rights are reserved, including those for text and data mining, AI training, and similar technologies.

these events, stringent and temporally focused emission control measures were implemented in Beijing and its surrounding regions. These actions primarily included temporary shutdowns or reduced output of industrial sources and traffic restrictions, introduced under a coordinated, cross-regional framework. VOC concentrations also showed significant decreases during the events (Li et al., 2023c; Liu et al., 2024). For example, non-biogenic VOCs decreased by more than 40% during $APEC_{2014}$ (Li et al., 2017), and oxygenated organic molecules (OOMs) exhibited significantly lower concentrations during WOG_{2022} compared to the same periods in 2019 and 2021 (Guo et al., 2023). Changes in VOC levels also affect SOA formation potential and aging processes (Liu et al., 2021). In contrast, population mobility events represented by the Chinese New Year (CNY) involve large-scale, short-term outflows of residents and migrant workers from Beijing for holiday travel and family reunions, with a substantial portion of the urban population temporarily leaving the city (called Chunyun). As a result, daily urban activities including commuting, commercial operations, and industrial production are substantially reduced, leading to considerable decreases in primary pollutants such as nitrogen oxides (NO_x), carbon monoxide (CO) and cooking-related OA (COA), while secondary species may show slight decreases or occasional increases (Ren et al., 2025; Sun et al., 2020a). However, accurate evaluation of the impacts of emission changes on OA is still challenging because of the absence of integrated measurements of both OA and VOC precursors and the unclear chemical relationship between VOCs and SOA formation during these control periods.

Meteorological conditions are also important factors affecting mass concentrations of aerosol species. For example, the large decrease in PM concentrations during the 2008 Olympic Games was mainly caused by meteorological variability rather than emission changes (Tao et al., 2009). In contrast, Qu et al. (2024) found that the reductions in primary OA (POA) and aqueous-phase oxygenated OA (aqOOA) during WOG_{2022} were mainly due to emission reductions. However, despite substantial reductions in anthropogenic emissions during the coronavirus disease (COVID-19) lockdown in Beijing (Chang et al., 2023), certain meteorological conditions (e.g., low wind speed, high relative humidity) paradoxically caused a 119% increase in SOA mass concentrations. These findings highlight the combined influences of emission changes and meteorological conditions on PM variations, yet the relative contributions of these two factors to OA during such events have not been systematically evaluated.

In this study, six field datasets are analyzed to evaluate the impacts of short-term emission changes on OA during distinct episodes characterized by policy interventions and population mobility. The relative contributions of meteorological and emission effects to OA variations are quantified. Additionally, the impact of changes in VOCs on SOA formation potential and aging processes during WOG_{2022} are characterized.

2. Experimental methods

2.1. Field measurements

All measurements were conducted at the Tower Branch of the Institute of Atmospheric Physics (IAP), Chinese Academy of Sciences (39°58′28″ N, 116°22′16″ E). Three policy interventions ($APEC_{2014}$, $V\text{-}Day_{2015}$, and WOG_{2022}) and three population mobility events ($CNY_{2019–2021}$) were analyzed in this study, as detailed in previous publications (Li et al., 2025; Sun et al., 2020b; Sun et al., 2016; Xu et al., 2015; Zhao et al., 2017; Zhou et al., 2022). During the policy interventions, stringent and temporally focused emission control measures, which primarily included temporary industrial shutdowns or output reductions and traffic restrictions, were implemented in Beijing and its surrounding regions under a coordinated, cross-regional framework. In contrast, local emissions in Beijing decreased significantly during the CNY holiday owing to population outflow, while those in surrounding areas did not decrease correspondingly, making regional transport a relatively prominent contributor to pollutant levels in Beijing. The control period (4–20 February 2022) is defined as the WOG period, while the preceding period (19 January–3 February 2022) serves as the background reference period (before the WOG, BWOG). Detailed information on the defined analysis periods for other campaigns is provided in Table S1.

Non-refractory PM (NR-PM) species were measured using a High-Resolution Time-of-Flight Aerosol Mass Spectrometer (HR-ToF-AMS, Aerodyne, USA) or a Time-of-Flight Aerosol Chemical Speciation Monitor (ToF-ACSM, Aerodyne, USA) in different campaigns (Table S1). It should be noted that the ToF-ACSM was equipped with a capture vaporizer (CV), while the HR-ToF-AMS was equipped with a standard vaporizer (SV). To minimize the impact of vaporizer differences on source apportionment, we used the corresponding standard spectral libraries for positive matrix factorization (PMF) analysis (Hu et al., 2018a; Ulbrich et al., 2009). Despite the potential differences in measured aerosol properties due to the use of different vaporizers, strong temporal correlations were observed between the PMF factors derived from the two instruments (Hu et al., 2018b), indicating that the results are comparable. However, this vaporizer difference still introduces some uncertainty in cross-year comparisons. For the HR-ToF-AMS and ToF-ACSM measurements, the collection efficiency (CE) and relative ionization efficiency (RIE) applied in each campaign are summarized in Table S2.

Fig. S1 shows strong correlations (coefficient of determination, R^2 = 0.88–0.96) between NR-PM + black carbon (BC) and $PM_{2.5}$ at the Olympic Sports Center station across various events, although the fitted slopes were low (0.47–0.69). This discrepancy primarily stems from the difference in sampled size fractions (PM_1 vs. $PM_{2.5}$). Additional contributions to the deviation include fundamental differences in measurement methodology (β-ray absorption vs. HR-ToF-AMS/ToF-ACSM), as well as the assumption of a fixed CE value of 0.5, which introduces potential uncertainties. Finally, hygroscopic growth under high relative humidity may inhibit the effective transmission of larger particles by the HR-ToF-AMS, further exacerbating the underestimation. These slopes are similar to those of previous studies in other Chinese cities (Elser et al., 2016; Wang et al., 2015; Zhang et al., 2017).

During WOG_{2022}, an Oxidation Flow Reactor (OFR, Aerodyne, USA) along with a HR-ToF-AMS was deployed to investigate SOA formation and aging. The OFR was operated at OH exposures ranging from 1.94×10^{11} to 1.83×10^{12} mol cm^{-3} s, which were chosen to simulate approximately 1.8–3.0 equivalent days of atmospheric photochemical aging (Table S3). The sampling system used an automatic switching valve to alternate between two lines at 15-min intervals: (1) an ambient bypass line for direct sampling and (2) a line where ambient air was first drawn through a 15-cm copper inlet into the OFR for oxidation (with dilution by high-purity nitrogen gas), and then dried before being analyzed by the HR-ToF-AMS. This setup enabled quasi-synchronous measurement of both ambient aerosols and those subjected to controlled photochemical aging using the HR-ToF-AMS.

VOCs were measured online using a time-of-flight chemical ionization mass spectrometer (ToF-CIMS) with iodide (I^-) as the reagent ion in 2021 and 2022. Raw mass spectral data were processed using the Tofware software package implemented in Igor Pro. To minimize the influence of fluctuations in reagent ion intensity, all VOC signals were normalized to the I^- signal. Daily background measurements were conducted to subtract instrumental background signals, and quality control was applied based on the signal-to-noise ratio (S/N), with low S/N signals excluded and signals with higher uncertainty down-weighted. Instrumental settings were maintained consistently throughout the observation period, ensuring comparability of the VOC measurements across the entire study. For detailed methods, please refer to Li et al. (2025). These comprehensive and concurrent measurements of both aerosol components and gas-phase precursors during WOG_{2022} provide a unique dataset to investigate the mechanisms of SOA formation and reduction under stringent emission controls.

For the analysis of regional $PM_{2.5}$ and nitrogen dioxide (NO_2)

variations across the North China Plain, historical monitoring data were obtained from the national urban air quality real-time release platform of the China National Environmental Monitoring Centre (https://air.cnemc.cn:18007/). For each city, the change rate was calculated as the relative difference between the mean concentration during the event period and that during the adjacent reference period (Control time and Non-Control time as defined in Table S1). These publicly sourced $PM_{2.5}$ data are used exclusively for the regional-scale trend analysis presented here. Unless otherwise specified, all other aerosol data pertaining to chemical composition and source apportionment in this study are derived from the online instruments deployed at IAP tower observation site.

2.2. Source apportionment

For a direct comparison of OA composition between the 2021 and 2022 campaigns, the corresponding OA mass spectral datasets were merged and subjected to a unified PMF analysis (designated as $PMF_{2021+2022}$). The analysis was performed using the PMF2.exe algorithm (Zhang et al., 2015), which is based on Igor Pro and operated in robust mode (Paatero and Tapper, 1994). After evaluating solutions from 4 to 8 factors, a five-factor solution was selected as optimal, resolving two primary OA factors, namely COA and non-cooking OA (nCOA), along with three secondary OA factors, including oxidized primary OA (OPOA) and two oxygenated OA (OOA1 and OOA2). The selection was based on the mass spectral profiles, the correlations with external tracers, and the diurnal variation patterns. Detailed diagnostics, mass spectra, and time series for these five factors are provided in Text S1 and Fig. S2–S4. The robustness of this solution was further evaluated through bootstrap analysis (100 runs), with the derived factor uncertainties ranging from 0.13 to 0.71% (Fig. S5).

To investigate the aging processes of primary emissions and SOA formation under controlled oxidation, we analyzed the dataset combining ambient aerosols with those processed by the OFR during WOG_{2022}. The Multilinear Engine (ME-2) model was applied, using the mass spectral profiles of the five OA factors identified in the $PMF_{2021+2022}$ analysis as constraints to ensure consistency between ambient and OFR-processed data, thereby allowing direct comparison of SOA formation potential under varying oxidation conditions. As shown in Fig. S6, the time series of the constrained and ambient factors were well correlated. Full details of the method are provided in Text S2.

A second PMF analysis (PMF^2) (Petit et al., 2014) was applied to identify linkages between 182 VOC precursors (including 87 CHO and 95 CHNO compounds) and the formation of SOA. This analysis integrated the five OA factors from $PMF_{2021+2022}$, and VOC species measured online using ToF-CIMS during 2021 and 2022. All variables were normalized to their respective maximum values prior to analysis. The detailed analytical process, uncertainty treatment, and factor interpretation are provided in Text S3. An eight-factor solution was selected because it provided the clearest distinction between POA-dominated and SOA-related factors (Figure S7 and Figure S8). The robustness of this solution was further evaluated through bootstrap analysis (100 runs) (Fig. S9). In addition, details of source apportionment results from 2014 to 2020 can be found in previous studies (Lei et al., 2021b; Sun et al., 2020b; Sun et al., 2016; Xu et al., 2015; Zhao et al., 2017; Zhou et al., 2022).

2.3. Meteorological normalization using a machine learning model

The machine learning based Random Forest (RF) algorithm implemented in the R package rmweather (v0.1.2) (Grange and Carslaw, 2019) was used to eliminate the confounding effects of meteorological variables on gaseous and particulate pollutants. When constructing the RF prediction matrices for each event, we included explanatory variables such as aerosol components, OA factors, gaseous pollutants, and temporal variables including Unix time, Julian day, lunar day, day of the week, and hour (Zhou et al., 2022). Meteorological parameters included boundary layer height, total cloud cover, surface net solar radiation, total precipitation, and surface pressure from ERA5 reanalysis data, Hybrid Single-Particle Lagrangian Integrated Trajectory (HYSPLIT) backward trajectories, and meteorological parameters measured at 102 m. The dataset was randomly split into training and testing sets at a 7:3 ratio following Zhou et al. (2022), and model performance was evaluated by the coefficient of R^2 between predictions and observations on the test set. To derive meteorologically normalized concentrations, we applied a weather normalization procedure where the trained RF model was used to predict concentrations for each data point, but with its actual meteorological data replaced by values randomly resampled from the entire study period (while preserving the true temporal variables). This random resampling and prediction process was repeated 1000 times independently for each point, and the arithmetic mean of these predictions was taken as the de-weathered concentration. The resulting normalized time series thus primarily reflects variations driven by emission changes (integrating the effects of both local and regional sources) rather than specific meteorological conditions. As shown in Fig. S10, the RF predictions exhibited strong correlations with observations ($R^2 = 0.7–1.0$). The other set of performance metrics, root mean square error (RMSE), and the mean absolute error (MAE), for each species and event is provided in Supplementary Material (Table S4). Overall, the consistently high R^2 values and the low magnitude of prediction errors confirm the robust performance of the meteorological normalization models across all pollutants and events.

3. Results and discussion

3.1. Response of particulate matter and NO_2 pollution to emission changes

Aerosol species exhibit varying responses to different emission control scenarios. During policy interventions ($APEC_{2014}$, $V\text{-}Day_{2015}$, and WOG_{2022}), the total NR-PM measured by HR-ToF-AMS decreased by 50.1–62.9% (Fig. 2), which was greater than the 16–46% reduction reported for the CNY in previous years (e.g., as specifically reported for four separate years in Sun et al. (2020a), see also long-term trend analyses in Ren et al. (2025). Also, these policy interventions resulted in a region-wide decrease in $PM_{2.5}$ across the North China Plain, with pronounced spatial heterogeneity (Fig. 1). As the core control zone, Beijing showed the largest decrease in $PM_{2.5}$ by 51.9–71.2% during these three policy interventions ($APEC_{2014}$, $V\text{-}Day_{2015}$, and WOG_{2022}), while surrounding regions implementing coordinated controls such as Tianjin and Hebei also exhibited considerable reductions by 15.9–50.1% during $APEC_{2014}$, 11.5–70.7% during $V\text{-}Day_{2015}$, and 22.7–50.2% during WOG_{2022}, respectively. Although the reductions in Tianjin and Hebei were slightly lower than those in Beijing, they still highlight the effectiveness of regional joint prevention and control policies.

In contrast, during the CNY_{2019}, although a large fraction of population moved out of Beijing by approximately 46% for vacation and/or hometown-visit (https://www.qstheory.cn/laigao/ycjx/2019-02/14/c_1124115748.htm) and led to much reduced local anthropogenic activities, $PM_{2.5}$ concentrations in Beijing decreased by only 18.0%, which was much lower than the reductions observed in cities to its south, such as Baoding and Shijiazhuang (28.3–43.5%). This suggests spatial disparities in reduction efficiency in the absence of regional emission controls (Fig. 1), likely due to differences in local emission sources, meteorological conditions, and regional transport contributions. In contrast to $PM_{2.5}$, NO_2 concentrations showed a more uniform and large decrease across the region, with a 47.2% reduction in Beijing and 35.8–65.7% in surrounding provinces (Tianjin, Hebei, Shanxi, Shandong). Such decreases even exceeded the reductions observed during policy interventions (5.9–57.1%) (Fig. 1). The spatial distribution of NO_2 decrease was further supported by satellite-based tropospheric NO_2 vertical column density retrievals from the POMINO products (Lin et al.,

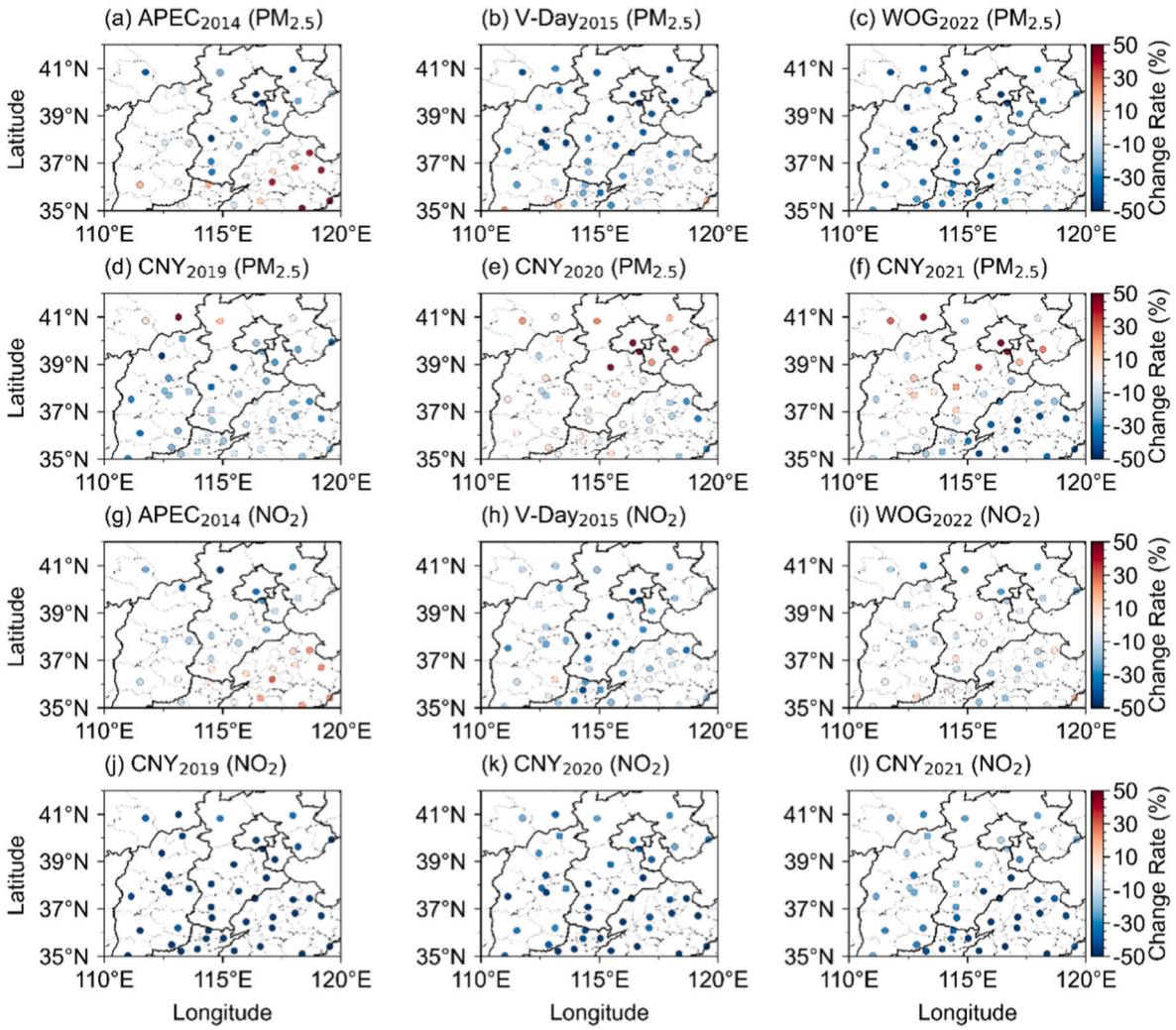


Fig. 1. $PM_{2.5}$ and NO_2 concentration change rates (%) during six events in North China. (a, g) $APEC_{2014}$, (b, h) $V\text{-}Day_{2015}$, (c, i) WOG_{2022}, (d, j) CNY_{2019}, (e, k) CNY_{2020}, (f, l) CNY_{2021}. Red/blue indicates an increase/decrease in concentration change rates during the event. (For interpretation of the references to color in this figure legend, the reader is referred to the Web version of this article.)

2015; Lin et al., 2014; Liu et al., 2019; Liu et al., 2020) (Fig. S11). The large decreases in NO_2 concentrations during the CNY_{2019} are consistent with the fact that traffic emissions were largely reduced during the spring festival holiday.

By comparison, the CNY_{2020} and CNY_{2021} coincided with COVID-19 containment measures, which limited population mobility and social activities, presenting emission scenarios distinct from those in 2019. During these periods, NR-PM mass concentrations in Beijing increased by 19.4–84.7% (Table S5), and $PM_{2.5}$ levels rose by 58.2–81.6%, with increases notably higher than those in surrounding cities (Fig. 1). Meanwhile, NO_2 concentrations decreased by 13.8% and 58.2% during the CNY_{2020} and CNY_{2021} respectively (Fig. 1). These patterns differed from those observed during the CNY_{2019}, likely because the benefits of local emission reductions achieved during the lockdowns were offset by unfavorable meteorological conditions and an enhanced atmospheric oxidative capacity, which led to increased secondary production (Chang et al., 2023; Sun et al., 2020a). Notably, while WOG_{2022} also coincided with pandemic-related restrictions. However, the concurrent implementation of targeted, regionally coordinated emission controls likely led to its more substantial air quality improvements.

3.2. Response of aerosol species to emission changes

As shown in Fig. 2, OA concentrations decreased by 32.8–51.4% under the three policy interventions, which were smaller than the 59.2–77.1% reductions in secondary inorganic aerosol (SIA). SOA typically dominates the larger accumulation mode compared to POA. During the study period, SOA showed a significantly larger reduction than POA (46.3–63.7% vs. 16.9–39.7%), highlighting the important role of emission controls in Beijing and surrounding regions in reducing secondary aerosol levels. The smaller decrease in POA probably resulted from less stringent controls on local emissions near the sampling site.

In contrast, population mobility events ($CNY_{2019–2021}$) resulted in a more significant decrease in POA (25.9%) compared to SOA (−56.9%), with POA reductions ranging from 1.1% to 48.1% and SOA changes ranging from −148.0% to 7.1%. The large fluctuations may be attributed to differences in meteorological conditions and regional transport across the three CNY events, as well as the confounding effects of COVID-19 control measures. These events were primarily driven by changes in local emissions resulting from short-term population migration during the holiday, rather than by policy-induced regional emission controls. A notable portion of population mobility during the CNY period likely involves short-distance to medium-distance relocations, especially to nearby provinces. This suggests that regional emissions associated with population activity may either remain largely unchanged or even increase to some extent in the provinces surrounding Beijing (e.g., Hebei, Tianjin, Shanxi). Under such conditions, regional transport combined with unfavorable meteorology can partly counteract

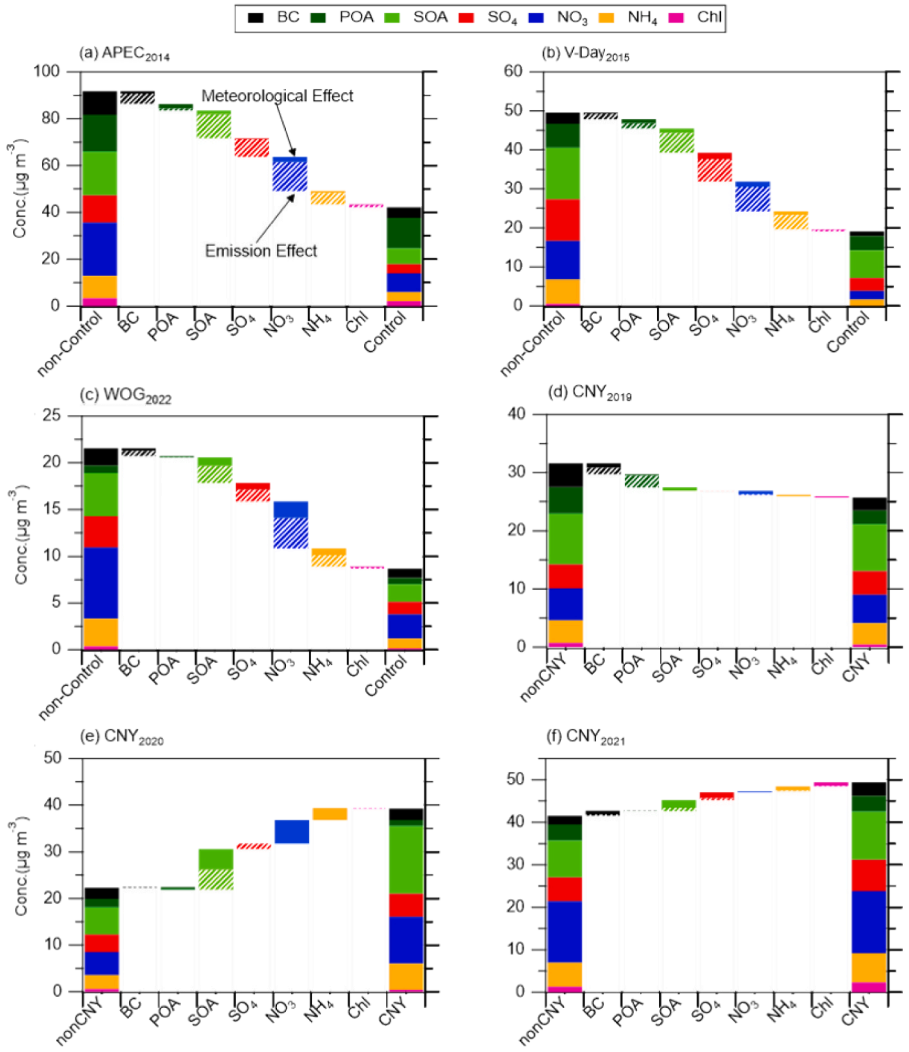


Fig. 2. Changes in PM species concentrations under (a)$APEC_{2014}$, (b)$V\text{-}Day_{2015}$, (c)WOG_{2022}, (d) CNY_{2019}, (e) CNY_{2020}, (f) CNY_{2021}. Pollution concentrations were measured at the IAP tower site. The figure illustrates how PM species concentrations evolve from the pre-control period to the non-control period under the combined influence of meteorological and emission effects.

the benefits of local emission controls in Beijing. Detailed changes in mass concentrations of PM species and gaseous pollutants are presented in Table S5. Note that this comparison may introduce uncertainty, as the CV vaporizer used in the $CNY_{2019–2020}$ campaigns is known to yield higher SOA fractions than the SV used in 2021 (Zheng et al., 2020).

Further analysis of the size distributions revealed a consistent shift in the OA peak diameters from larger sizes (600–700 nm) to smaller sizes (400–500 nm) during control periods (Fig. S12). This result indicates that the larger-sized OA fraction was more effectively suppressed. Since SOA is typically more abundant in the larger accumulation mode relative to POA (Xu et al., 2021), the observed shift implies a relatively larger decrease in SOA mass, consistent with the more pronounced reduction in SOA compared to POA (Fig. 2). This suppression is likely due to reduced precursor availability. While direct VOC measurements were unavailable for $APEC_{2014}$ and $V\text{-}Day_{2015}$, previous studies have documented significant reductions in non-biogenic VOCs and oxygenated organic molecules during such control periods (Guo et al., 2023; Li et al., 2017). The observations during WOG_{2022} (Section 3.2) further confirmed this. Additionally, the reduction may also be linked to POA, as a portion of SOA originates from its oxidation. This is supported by the substantial decrease (61.7%) in the POA-related OPOA resolved by PMF analysis during the WOG period.

The contributions of emission effects and meteorological effects to the observed changes of aerosol species are shown in Figs. 2 and 3. Note that emission effects denote the net influence of changes in both local and regional emissions after removing the influence of meteorological conditions. During the three policy interventions, emission effects accounted for 62.9–74.0% and 65.6–86.1% of the decreases in OA and SOA concentrations in Beijing, respectively. This contribution far exceeded that from meteorological effects, confirming that emission controls were the dominant driver of SOA reductions during these periods. In contrast, during the population mobility events, meteorological effects played a substantially larger role in driving SOA concentration changes through their influence on pollutant accumulation and dispersion. For example, during the CNY_{2019}, favorable meteorology facilitated SOA dispersion, while during the CNY_{2020} and CNY_{2021}, unfavorable meteorological conditions promoted pollutant accumulation, leading to increases in SOA concentrations (50.9–72.7%). This finding is consistent with the mechanism identified during the COVID-19 lockdown, where unfavorable meteorological conditions increased both POA and SOA concentrations, with a substantially greater impact on SOA, which ultimately resulted in its net increase despite concurrent emission reductions (Chang et al., 2023). These results indicate that SOA reductions were less pronounced during the population mobility events than during policy interventions, as the decline in local emissions in Beijing during those periods was insufficient to offset the impact of

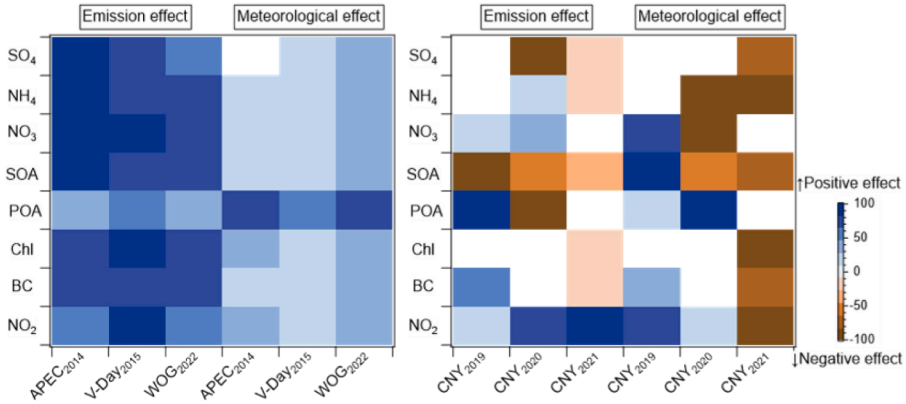


Fig. 3. Contributions of emission effects and meteorological effects to changes in mass concentrations of PM species and NO_2. Pollution concentrations were measured at the IAP tower site. Positive values indicate contributions to concentration decreases, while negative values indicate contributions to concentration accumulation.

unfavorable meteorological conditions on SOA formation (Chen et al., 2023; Liu et al., 2025).

Compared to SOA, POA exhibited distinct sensitivities to short-term emission variations. Under policy interventions, POA was more strongly influenced by meteorological effects (45.6–72.3%) than by emission effects (27.7–54.4%). In contrast, during the CNY_{2019} and CNY_{2021}, the reduction in POA was primarily driven by emission effects. However, during the CNY_{2020}, meteorological effects had a significant impact on POA levels, likely due to the stringent mobility restrictions implemented to prevent the spread of COVID-19 virus during that year. It is worth noting that WOG_{2022} coincided with both CNY holiday and the zero-COVID policy. While these potential factors may have exerted certain

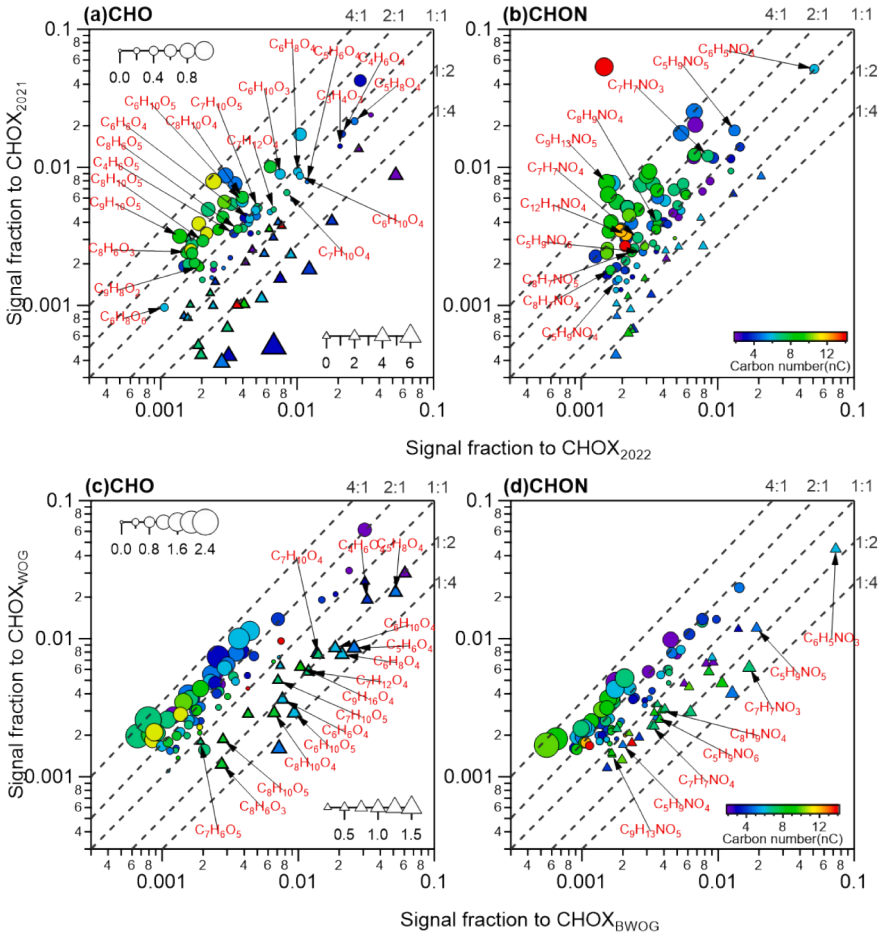


Fig. 4. Comparison of mean mass spectra of CHO and CHON compounds. Panels (a–b) show the comparison of signals during WOG_{2022} versus the same period in 2021. Panels (c–d) show the comparison within WOG_{2022}, divided into the BWOG and the WOG periods. Marker size is proportional to the fractional difference in ion signal, and color indicates the number of carbon atoms. Circles indicate higher signal levels during the WOG compared to BWOG period, or higher signal levels in 2021 compared to 2022, while triangles represent the opposite. (For interpretation of the references to color in this figure legend, the reader is referred to the Web version of this article.)

influences on emissions, they are insufficient to account for the substantial SOA reductions observed during the WOG period. As demonstrated in previous studies, emission controls specific to the WOG period were the primary driver of the improved air quality at that time (Jiang et al., 2024; Qu et al., 2024).

3.3. Changes of VOCs during the control period

Despite substantial reductions in PM concentrations during the WOG period, the total VOC signals showed little change between the BWOG and WOG periods (253.5 ions s^{-1} vs. 266.4 ions s^{-1}), probably reflecting the earlier implementation of short-term restrictions on industrial activities in surrounding provinces with significant VOC emissions (e.g., https://www.szx.gov.cn/xxgk_21446/zfxxgk/fdzdgknr/zfwj/szbf/202111/t20211112_1073449.html).

However, noticeable changes in specific gaseous compounds were still observed during the WOG period (Fig. 4). For example, levoglucosan ($C_6H_{10}O_5$) decreased by 67.4%, while several other compounds identified as dicarboxylic acids (e.g., $C_5H_6O_4$, $C_6H_6O_4$, $C_8H_{10}O_4$) and nitrophenols (e.g., $C_6H_5NO_3$, $C_7H_7NO_3$) showed reductions of approximately 50%. These dicarboxylic acids and nitrophenols can originate from biomass burning or from the atmospheric oxidation of anthropogenic aromatic compounds emitted by traffic and industry (Ahmed et al., 2023; Leppla et al., 2026; Molteni et al., 2018; Zheng et al., 2023b; Zhou et al., 2024). Although some of these compounds, such as $C_5H_6O_4$, may also have biogenic sources, as shown by isoprene photooxidation experiments (Nguyen et al., 2011), their observed decreases in urban areas likely reflect effective controls on anthropogenic emissions. A detailed summary of the identification of these compounds and their proposed sources, along with supporting references, is provided in Table S6. The decrease in primary aerosol components such as POA and BC during the WOG period (16.9–45.6%) is consistent with the reductions reported for $APEC_{2014}$ and $V\text{-}Day_{2015}$ (Li et al., 2016b; Yang et al., 2016).

Concurrently, oxygenated VOCs exhibited a differential response to precursor reduction. For example, compounds such as $C_4H_6O_4$, $C_5H_8O_4$, $C_6H_{10}O_4$, $C_7H_{12}O_4$, $C_7H_7NO_4$, $C_8H_{10}O_4$, and $C_8H_{10}O_5$, which have been linked to biomass burning and the oxidation of anthropogenic aromatic emissions from traffic and industrial activities (Iinuma et al., 2010; Mochida et al., 2003; Molteni et al., 2018; Zhou et al., 2024) showed substantial reductions approximately 24.7–56.0%. Although some of these species may also receive contributions from biogenic sources (e.g., $C_5H_8O_4$, $C_6H_{10}O_4$ and $C_8H_{10}O_5$) (Jiang et al., 2025; Ye et al., 2021), their decreases were more pronounced than those observed for oxygenated VOCs more strongly associated with biogenic oxidation pathways, such as $C_5H_9NO_4$, $C_5H_9NO_5$, and $C_5H_9NO_6$ (10.1–34.7%) (Lee et al., 2014; Wu et al., 2021; Ye et al., 2021). Collectively, this pattern further indicates that the emission controls differentially affected the formation of various secondary VOC products, with a possible greater suppression observed for those more associated with anthropogenic precursors.

The volatility distributions of VOCs calculated following Li et al. (2016c) are shown in Fig. S13 (Text S4). The intermediate VOCs (IVOCs) accounted for 71.3% of the total VOCs during WOG_{2022}, a proportion comparable to that observed in Guangzhou during autumn (Chen et al., 2024b), but substantially higher than that in winter in Hong Kong (Nie et al., 2022), likely due to differences in meteorological conditions and emissions. Compared to the BWOG period, the IVOCs fraction further decreased during the WOG period (from 74.9% to 68.3%), while the semi-VOCs (SVOCs)/IVOCs ratio increased (0.27 vs. 0.35), indicating a reduction in the overall volatility of gaseous precursors. Meanwhile, the mean carbon oxidation state ($OSc = 2n_O/n_C - n_H/n_C$) decreased from 0.07 to −0.04 during the WOG period compared to the BWOG period, suggesting that the precursors were less oxidized under policy interventions, reflecting a larger contribution from freshly emitted compounds, which could affect their gas-to-particle partitioning behavior (Feng et al., 2023; Sun et al., 2025). It should be noted that the I-CIMS used in this study is primarily sensitive to relatively high-volatility VOCs (Price et al., 2021; Riva et al., 2019), thus the contributions from low-volatility VOCs (LVOCs) are likely underestimated, and the volatility distribution presented here may not fully capture the complete spectrum of SOA precursors.

To elucidate the influence of the policy interventions, WOG_{2022} was analyzed alongside the corresponding period in 2021. A substantial reduction in total signal intensity in 2022 was observed (261.7 ± 120.7 ions s^{-1} vs. 456.9 ± 199.4 ions s^{-1}), thus confirming the significant impact of the control measures. The mean molecular formula shifted from $C_{6.18}H_{9.84}O_{3.76}N_{0.57}$ in 2021 to $C_{5.28}H_{7.48}O_{3.91}N_{0.43}$ in 2022, with oxygen-carbon ratio (O/C) increasing from 0.56 to 0.65. The increase in O/C and the decreases in carbon and nitrogen numbers in 2022 compared to 2021 may reflect a combination of factors, including reduced fresh emissions due to sustained emission controls and the potential influence of more aged air masses from regional transport. This shift in molecular composition may affect the subsequent atmospheric processing of VOCs. Specifically, CHON-VOCs decreased by 57.2%, while CHO-VOCs only declined by 23.2%, highlighting the compound-dependent effects of emission control measures. This divergence is likely driven by the 70.3% reduction in NO_x emissions in 2022, which likely suppressed NO_x-driven formation of nitrogen-containing VOCs. Consistent with these trends, specific tracers such as adipic acid ($C_6H_{10}O_4$, typically associated with COA (Reyes-Villegas et al., 2018)) and levoglucosan decreased by 25.3% and 57.3%, respectively, consistent with the decreases in COA and nCOA (75.1% and 80.4%, respectively), further supporting the effectiveness of emission control measures. Additionally, dicarboxylic acids such as $C_5H_8O_4$ and $C_4H_6O_4$ showed signal intensity reductions of 20–40%, compounds likely derived from aromatic oxidation, including $C_8H_{10}O_5$ and $C_8H_{10}O_4$, as well as nitrophenols (e.g., $C_7H_7NO_3$, $C_7H_7NO_4$, $C_6H_5NO_3$) showed greater decreases (30–60%). The similarity of these species to those showing pronounced decreases during the WOG period further highlights the effectiveness of emission controls on VOCs predominantly associated with anthropogenic sources.

3.4. Contribution of VOCs to SOA

Fig. 5 illustrates the contribution of CHO and CHON compounds to the formation of SOA. During 2021–2022, CHO-VOCs contributed predominantly to OOA2 (49.2–60.0%), whereas CHON-VOCs showed higher contributions to OOA1 (23.6–34.5%) and OPOA (40.7–41.9%). IVOCs played a dominant role in SOA formation, contributing 83.4–84.0% of the SOA from CHO-VOCs and 54.9–62.4% from CHON-VOCs, respectively, consistent with previous studies (Hu et al., 2022; Shen et al., 2023). However, the ratio of IVOCs-to-SVOCs contributions to SOA formation in CHON-VOCs was significantly lower than that in CHO-VOCs (1.3–1.7 vs. 11.4–11.9). This suggests that while IVOCs are the primary contributors, SVOCs in CHON-VOCs also play an important role in SOA formation.

Policy interventions altered the composition of gaseous precursors, subsequently shifting their contribution to SOA formation. Specifically, the contribution of CHO-VOCs to OOA2 decreased from 72.4% during the BWOG period to 52.7% during the WOG period, while their contributions to OOA1 and OPOA increased from 10.3 to 21.9% and from 17.3 to 25.5%, respectively. A similar pattern was observed for CHON-VOCs: their contribution to OOA2 decreased from 42.6 to 30.5%, while their contributions to OOA1 (20.9–36.6%) and OPOA (25.0–44.5%) increased. When comparing the data from 2021 to 2022, the trends were reversed. The contribution of CHO-VOCs and CHON-VOCs to OOA2 increased in 2022 (34.5–60.0%) compared to the same period in 2021 (24.8–49.2%), while their contribution to OOA1 decreased from 26.5–34.5% to 17.6–23.6%. These changes suggest that the policy interventions in 2022 had a different impact on the contribution of VOCs to SOA formation compared to 2021.

Fig. S14 shows that the reductions in OOA2 and OPOA mass concentrations (36.5–59.5%) in 2022 were comparable to the decreases

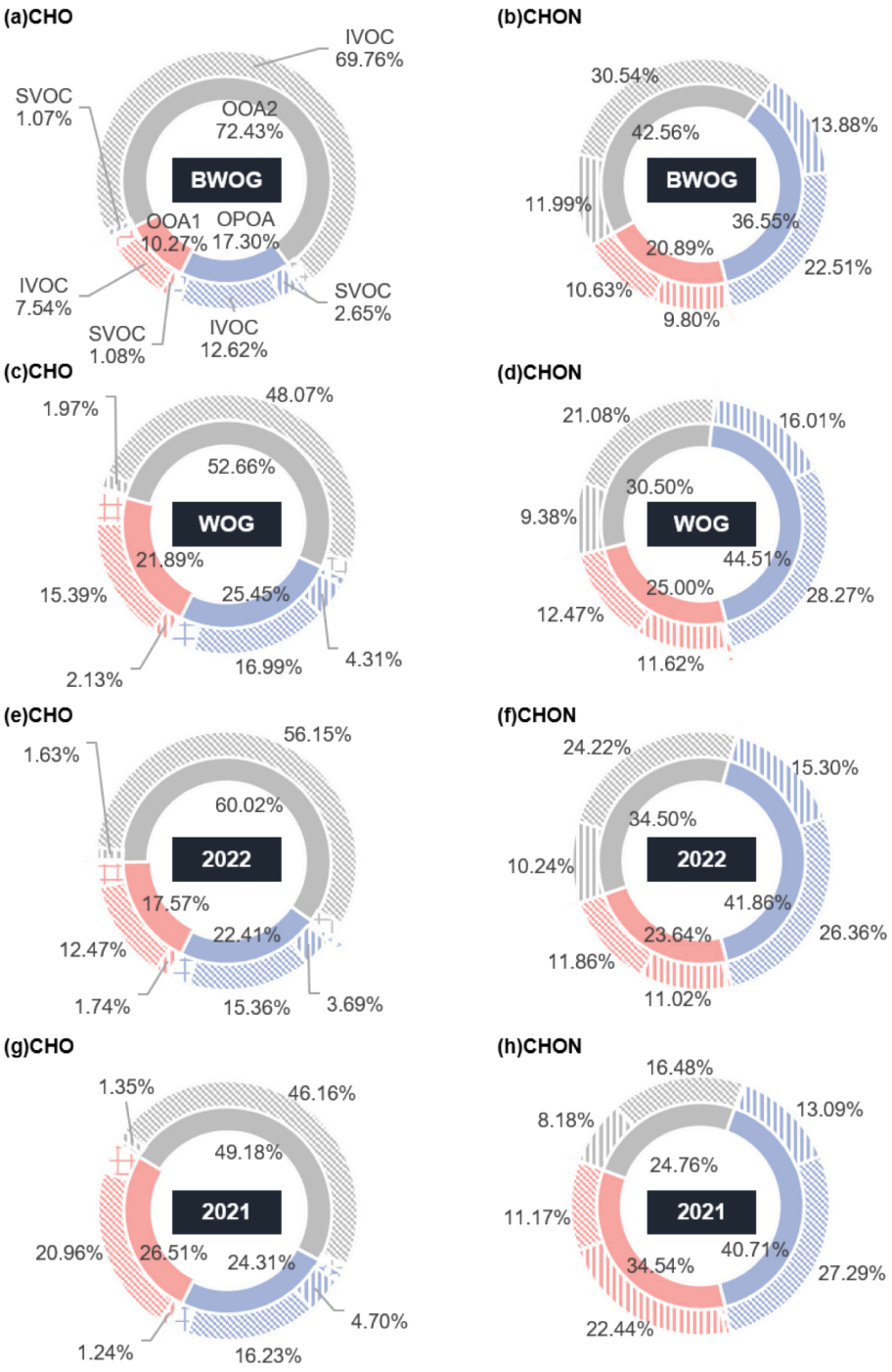


Fig. 5. Contribution of (a, c, e, g) CHO-VOCs and (b, d, f, h) CHON-VOCs compounds to OOA1, OOA2, and OPOA for (a, b) BWOG, (c, d) WOG, and (e, f) winters of 2022 and (g, h) 2021.

observed for their respective precursor VOCs (20.5–62.6%). In contrast, the decreases in mass concentration of OOA2 and OPOA during the WOG period were much higher than their precursors (58.5–61.7% vs. −26.2–37.6%) compared to the BWOG period. These discrepancies suggest that SOA formation was more sensitive to precursor changes during the policy interventions, altering the pathways through which precursors contribute to SOA formation. In addition, while OOA1 mass concentration in 2022 showed a dramatic 98.5% reduction compared to 2021, its precursor compounds, CHO-VOCs and CHON-VOCs, only decreased by 75.1% and 56.9%, respectively. This indicates that OOA1 formation is highly sensitive to precursor variations, leading to substantial reductions even with initial declines in precursor concentrations. Notably, the mass concentration of OOA1 remained at very low levels (<0.1 μg m^{-3}) with negligible change between the WOG and BWOG periods, further suggesting that OOA1 formation is particularly sensitive to precursor availability.

3.5. Changes of SOA formation and aging processes

The mass concentrations of OA components varied distinctly with photochemical aging during WOG_{2022}. As shown in Fig. 6, POA mass concentration decreased by 0.2–0.3 μg m^{-3} after 1.5 equivalent days and then stabilized. This decrease is likely due to particle fragmentation induced by heterogeneous oxidation, consistent with previous chamber

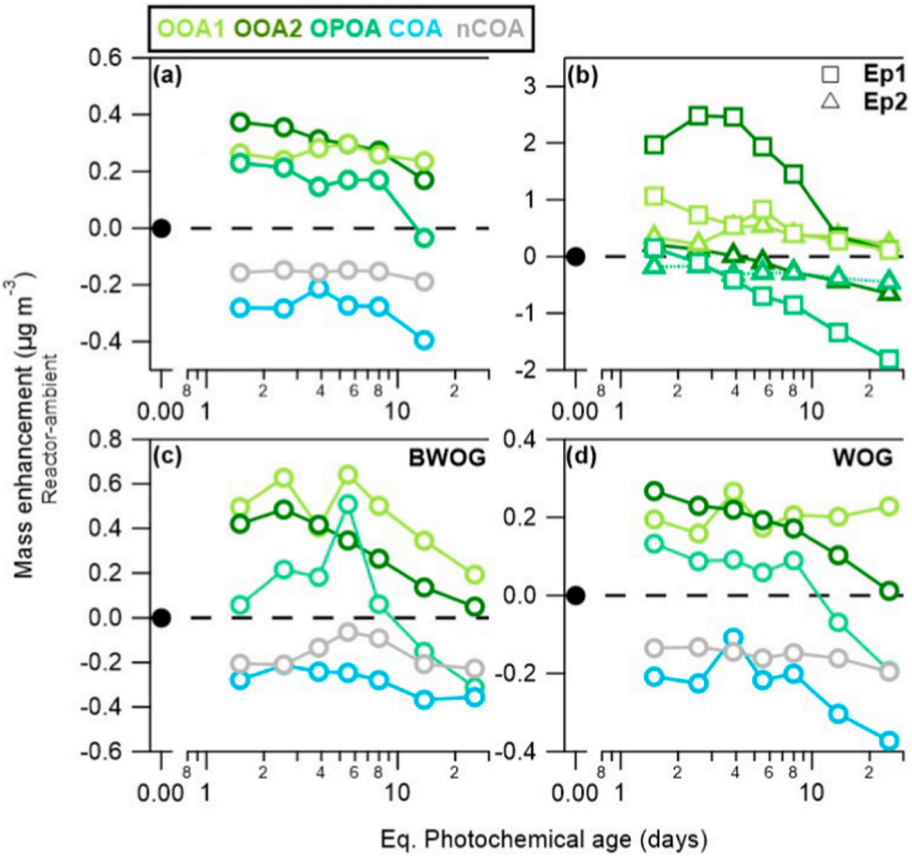


Fig. 6. Absolute enhancement of the mass concentration as a function of photochemical age for (a) entire period in 2022, (b) Ep1 and Ep2, (c) BWOG, and (d) WOG.

experiments and field observations (Asa-Awuku et al., 2009; Xu et al., 2022; Zhang et al., 2024). In contrast, SOA concentrations generally exhibited increases (0.2–0.4 μg m^{-3}). However, this increase was lower than that observed in summer in Beijing, possibly due to lower biogenic VOC emissions in winter (Zhang et al., 2024) which are limited by cold ambient temperatures and restrict SOA formation (Saha et al., 2018).

The aging processes of SOA components differed significantly between the WOG and BWOG periods. OOA1 exhibited maximum mass increment during the BWOG period (0.6 μg m^{-3} at 5.5 days), while it reached only 0.3 μg m^{-3} after 3.9 days during the WOG period. Similarly, OOA2 exhibited a smaller maximum mass increase during the WOG compared to the BWOG period (0.3 vs. 0.5 μg m^{-3}), with the equivalent aging time substantially shortened from 2.6 to 1.5 days. The maximum mass increase of OPOA dropped sharply from 0.5 μg m^{-3} at 5.5 days during the BWOG period to 0.1 μg m^{-3} at 1.5 days during the WOG period. Interestingly, the maximum increase in the O/C ratio due to photochemical aging was more pronounced during the WOG period, indicating a faster oxidation rate of SOA under policy interventions (Fig. S15), likely due to the lower initial oxidation state of the precursors during this period. The increase in nitrogen-to-carbon ratio (N/C) was also more significant during the WOG period (0.005 vs. 0.003), likely due to increased fraction of CHON-VOCs compounds during the WOG period (43.8% vs. 41.8%). Variations in precursor components could thus account for the observed discrepancies in nitrogen-containing OA formation. These results demonstrate that policy interventions not only suppress SOA formation but also facilitate the aging process required to reach peak SOA mass concentrations.

To further investigate SOA formation and aging during different pollution episodes, we conducted a comparative analysis of SOA dynamics during the polluted events (Ep1 during the BWOG and Ep2 during the WOG period, Fig. S16), and the clean events (C1 during the BWOG and C2 during the WOG period). The exact dates and definitions for these specific polluted and clean analysis periods (Ep1, Ep2, C1, C2) are provided in Table S1. Detailed VOC component characteristics are provided in Table S7. As shown in Fig. 6, both OOA1 and OOA2 showed significant increases with photochemical aging, reaching maximum mass increments of 1.1 μg m^{-3} and 2.5 μg m^{-3} at 1.5 and 2.6 equivalent days, respectively, during Ep1. These increments were much higher than those observed during Ep2 (0.5 μg m^{-3} and 0.2 μg m^{-3} at 1.5 days). The discrepancies between Ep1 and Ep2 are likely driven by higher total precursor availability (407.9 ions s^{-1} vs. 340.3 ions s^{-1}) and POA levels (3.7 μg m^{-3} vs. 1.3 μg m^{-3}) during Ep1. In addition, several VOCs associated with anthropogenic emissions and secondary oxidation products, including levoglucosan, nitrophenols, and dicarboxylic acids, exhibited pronounced reductions during the WOG period (Fig. S17). The reduced abundance of these reactive VOC species during Ep2 likely limited SOA formation and subsequent aging, resulting in weaker SOA mass enhancement compared to Ep1. Although the overall SOA formation potential was lower on clean days compared to polluted days, SOA during C1 still showed a greater mass enhancement than that observed in C2 (Fig. S18).

4. Limitations

Several uncertainties in this study should be acknowledged. First, the $CNY_{2019–2020}$ (CV-ToF-ACSM, $PM_{2.5}$) and CNY_{2021} (SV-HR-ToF-AMS, PM_1) comparison introduces uncertainty, as the vaporizer difference (CV vs. SV) significantly affects organic factors (higher SOA fractions for CV), and the particle size discrepancy ($PM_{2.5}$ vs. PM_1) adds additional uncertainty, despite the good correlation observed between $PM_{2.5}$ and PM_1. Secondly, the mass non-closure between NR-PM + BC and $PM_{2.5}$ measured by independent instruments introduces an uncertainty into mass quantification, although their mass concentrations exhibit strong correlation. Furthermore, the PMF^2 approach introduces uncertainties,

as normalizing variables to maximum values eliminates unit differences but ignores relative weights, potentially obscuring the role of high-concentration SOA precursors. Additionally, time lags between measured VOCs and SOA caused by multi-generational oxidation may decouple their relationship, while the incomplete coverage of the ToF-CIMS (iodide reagent) over the full volatility range may bias the assessment of total precursor contributions, resulting in an underestimation of the contributions from the missing volatile fractions.

5. Conclusions

This study systematically evaluated the impacts of short-term emission changes on SOA in Beijing, comparing the effectiveness of regional coordinated controls (involving both local and regional emission reductions) with that of temporary population mobility restrictions. We demonstrate that the coordinated controls reduced SOA by 46.3–63.7%, with emission effects contributing 65.6–86.1% to this reduction—far exceeding the influence of meteorological effects. In contrast, SOA concentrations during the population mobility events were primarily governed by meteorological conditions. During WOG_{2022}, emission reductions not only decreased overall VOC precursor levels, especially those linked to anthropogenic activities (e.g., traffic-related and industry-related aromatic oxidation and biomass burning), but also modified their photochemical aging pathways. Results from oxidation flow reactor experiments indicated that the maximum SOA mass enhancement during photochemical aging decreased by a factor of 2–3 during the WOG period, with a markedly shorter equivalent aging time, highlighting that limited precursor availability constrained SOA formation and aging.

These results indicate that sustained and effective SOA mitigation requires coordinated control of precursors at the regional scale, especially key VOC components, which not only reduces emission intensity but also suppresses SOA formation and accumulation at the source. In contrast, temporary population mobility events represented by the Chunyun only reduce local emissions, and SOA reductions are limited and unstable when regional transport persists or meteorological conditions favor pollutant accumulation. These findings provide critical scientific support for targeted policies aiming at continuous improvement of regional air quality.

CRediT authorship contribution statement

Yu Zhang: Writing – original draft, Visualization, Software, Methodology, Formal analysis, Data curation. **Weiqi Xu:** Writing – review & editing, Methodology. **Wei Zhou:** Methodology, Data curation. **Jintai Lin:** Writing – review & editing, Validation, Methodology. **Mengying Wang:** Data curation. **Yan Li:** Resources, Data curation. **Siqi Zeng:** Resources, Data curation. **Ziyi Zhang:** Investigation, Data curation. **Xiaomin Cheng:** Investigation. **Yang Yang:** Investigation. **Yele Sun:** Writing – review & editing, Funding acquisition.

Notes

The authors declare that they have no conflict of interest.

Declaration of competing interest

The authors declare the following financial interests/personal relationships which may be considered as potential competing interests: Yele Sun reports financial support was provided by National Key Research and Development Program of China (No. 2024YFC3711900). Yele Sun reports financial support was provided by Strategic Priority Research Program of the Chinese Academy of Sciences (Grant No. XDB0760200). If there are other authors, they declare that they have no known competing financial interests or personal relationships that could have appeared to influence the work reported in this paper.

Acknowledgements

This work was supported by the National Key Research and Development Program of China (No. 2024YFC3711900) and the Strategic Priority Research Program of the Chinese Academy of Sciences (Grant No. XDB0760200).

Appendix A. Supplementary data

Supplementary data to this article can be found online at https://doi.org/10.1016/j.envpol.2026.128408.

Data availability

Data will be made available on request.

References

Ahmed, M., Rappenglueck, B., Ganranoo, L., Dasgupta, P.K., 2023. Source apportionment of gaseous Nitrophenols and their contribution to HONO formation in an urban area. Chemosphere 338, 139499.

Asa-Awuku, A., Miracolo, M.A., Kroll, J.H., Robinson, A.L., Donahue, N.M., 2009. Mixing and phase partitioning of primary and secondary organic aerosols. Geophys. Res. Lett. 36, L15827.

Chang, X., Zheng, H.T., Zhao, B., Yan, C., Jiang, Y.Q., Hu, R.L., Song, S.J., Dong, Z.X., Li, S.Y., Li, Z.Q., Zhu, Y., Shi, H.R., Jiang, Z., Xing, J., Wang, S.X., 2023. Drivers of high concentrations of secondary organic aerosols in Northern China during the COVID-19 lockdowns. Environ. Sci. Technol. 57, 5521–5531.

Chen, L., Liao, H., Li, K., Zhu, J., Long, Z.Y., Yue, X., Yang, Y., Zhang, M.G., 2023. Process-Level quantification on opposite $PM_{2.5}$ changes during the COVID-19 lockdown over the North China Plain. Environ. Sci. Technol. Lett. 10, 779–785.

Chen, Q., Miao, R.Q., Geng, G.N., Shrivastava, M., Dao, X., Xu, B.Y., Sun, J.Q., Zhang, X., Liu, M.Y., Tang, G.G., Tang, Q., Hu, H.W., Huang, R.J., Wang, H., Zheng, Y., Qin, Y., Guo, S., Hu, M., Zhu, T., 2024a. Widespread 2013-2020 decreases and reduction challenges of organic aerosol in China. Nat. Commun. 15, 4465.

Chen, W., Hu, W.W., Tao, Z., Cai, Y.Y., Cai, M.F., Zhu, M., Ye, Y.Q., Zhou, H.S., Jiang, H. X., Li, J., Song, W., Zhou, J.Y., Huang, S., Yuan, B., Shao, M., Feng, Q.D., Li, Y., Isaacman-VanWertz, G., Stark, H., Day, D.A., Campuzano-Jost, P., Jimenez, J.L., Wang, X.M., 2024b. Quantitative characterization of the volatility distribution of organic aerosols in a polluted urban area: intercomparison between thermodenuder and molecular measurements. J. Geophys. Res. Atmos. 129 e2023JD040284.

Elser, M., Huang, R.-J., Wolf, R., Slowik, J.G., Wang, Q., Canonaco, F., Li, G., Bozzetti, C., Daellenbach, K.R., Huang, Y., Zhang, R., Li, Z., Cao, J., Baltensperger, U., El-Haddad, I., Prevot, A.S.H., 2016. New insights into $PM_{2.5}$ chemical composition and sources in two major cities in China during extreme haze events using aerosol mass spectrometry. Atmos. Chem. Phys. 16, 3207–3225.

Feng, T.T., Wang, Y.K., Hu, W.W., Zhu, M., Song, W., Chen, W., Sang, Y.Y., Fang, Z., Deng, W., Fang, H., Yu, X., Wu, C., Yuan, B., Huang, S., Shao, M., Huang, X.F., He, L. Y., Lee, Y.R., Huey, L.G., Canonaco, F., Prevot, A.S.H., Wang, X.M., 2023. Impact of aging on the sources, volatility, and viscosity of organic aerosols in Chinese outflows. Atmos. Chem. Phys. 23, 611–636.

Geng, G.N., Liu, Y.X., Liu, Y., Liu, S.G., Cheng, J., Yan, L., Wu, N.N., Hu, H.W., Tong, D., Zheng, B., Yin, Z.C., He, K.B., Zhang, Q., 2024. Efficacy of China's clean air actions to tackle $PM_{2.5}$ pollution between 2013 and 2020. Nat. Geosci. 17, 987–994.

Grange, S.K., Carslaw, D.C., 2019. Using meteorological normalisation to detect interventions in air quality time series. Sci. Total Environ. 653, 578–588.

Guo, Y.S., Deng, C.J., Ovaska, A., Zheng, F.X., Hua, C.J., Zhan, J.L., Li, Y.R., Wu, J., Wang, Z.C., Xie, J.L., Zhang, Y., Liu, T.Y., Zhang, Y.S., Song, B.Y., Ma, W., Liu, Y.C., Yan, C., Jiang, J.K., Kerminen, V.-M., Xia, M., Nieminen, T., Du, W., Kokkonen, T., Kulmala, M., 2023. Measurement report: the 4-year variability and influence of the Winter Olympicsand other special events on air quality in urban Beijing during wintertime. Atmos. Chem. Phys. 23, 6663–6690.

Hu, W., Day, D.A., Campuzano-Jost, P., Nault, B.A., Park, T., Lee, T., Croteau, P., Canagaratna, M.R., Jayne, J.T., Worsnop, D.R., Jimenez, J.L., 2018b. Evaluation of the new capture vaporizer for Aerosol Mass Spectrometers (AMS): elemental composition and source apportionment of Organic Aerosols (OA). ACS Earth Space Chem. 2, 410–421.

Hu, W., Zhou, H., Chen, W., Ye, Y., Pan, T., Wang, Y., Song, W., Zhang, H., Deng, W., Zhu, M., Wang, C., Wu, C., Ye, C., Wang, Z., Yuan, B., Huang, S., Shao, M., Peng, Z., Day, D.A., Campuzano-Jost, P., Lambe, A.T., Worsnop, D.R., Jimenez, J.L., Wang, X., 2022. Oxidation flow reactor results in a Chinese megacity emphasize the important contribution of S/IVOCs to Ambient SOA Formation. Environ. Sci. Technol. 56, 6880–6893.

Hu, W.W., Day, D.A., Campuzano-Jost, P., Nault, B.A., Park, T., Lee, T., Croteau, P., Canagaratna, M.R., Jayne, J.T., Worsnop, D.R., Jimenez, J.L., 2018a. Evaluation of the new capture vaporizer for aerosol mass spectrometers: characterization of organic aerosol mass spectra. Aerosol. Sci. Technol. 52, 725–739.

Iinuma, Y., Böge, O., Gräfe, R., Herrmann, H., 2010. Methyl-Nitrocatechols: atmospheric tracer compounds for biomass burning secondary organic aerosols. Environ. Sci. Technol. 44, 8453–8459.

Jiang, H., Deng, Y., Huo, Y., Wang, F., Chen, Y., Guo, H., 2025. Measurement report: molecular insights into organic aerosol sources and formation at a regional background site in South China. Atmos. Chem. Phys. 25, 13711–13727.
Jiang, Y.P., Yu, S.C., Chen, X., Zhang, Y.B., Li, M.Y., Li, Z., Song, Z., Li, P.F., Zhang, X.Y., Lichtfouse, E., Rosenfeld, D., 2024. Large contributions of emission reductions and meteorological conditions to the abatement of $PM_{2.5}$ in Beijing during the 24th Winter Olympic Games in 2022. J. Environ. Sci. 136, 172–188.
Kenagy, H.S., Heald, C.L., Tahsini, N., Goss, M.B., Kroll, J.H., 2024. Can we achieve atmospheric chemical environments in the laboratory? An integrated model-measurement approach to chamber SOA studies. Sci. Adv. 10 eado1482.
Lee, B.H., Lopez-Hilfiker, F.D., Mohr, C., Kurtén, T., Worsnop, D.R., Thornton, J.A., 2014. An iodide-adduct high-resolution time-of-flight chemical-ionization mass spectrometer: application to atmospheric inorganic and organic compounds. Environ. Sci. Technol. 48, 6309–6317.
Lei, L., Sun, Y.L., Ouyang, B., Qiu, Y.M., Xie, C.H., Tang, G.Q., Zhou, W., He, Y., Wang, Q. Q., Cheng, X.L., Fu, P.Q., Wang, Z.F., 2021b. Vertical distributions of primary and secondary aerosols in urban boundary layer: insights into sources, chemistry, and interaction with meteorology. Environ. Sci. Technol. 55, 4542–4552.
Lei, L., Zhou, W., Chen, C., He, Y., Li, Z.J., Sun, J.X., Tang, X., Fu, P.Q., Wang, Z.F., Sun, Y.L., 2021a. Long-term characterization of aerosol chemistry in cold season from 2013 to 2020 in Beijing, China. Environ. Pollut. 268, 115952.
Leppla, D., Hildmann, S., Zannoni, N., Kremper, L.A., Holanda, B.A., Williams, J., Pöhlker, C., Wolff, S., Sà, M., Solci, M.C., Pöschl, U., Hoffmann, T., 2026. Comprehensive non-targeted molecular characterization of organic aerosols in the Amazon rainforest. Atmos. Chem. Phys. 26, 365–390.
Li, H.Y., Zhang, Q., Duan, F.K., Zheng, B., He, K.B., 2016a. The "Parade Blue": effects of short-term emission control on aerosol chemistry. Faraday Discuss. 189, 317–335.
Li, J., Shi, Y.Q., Wu, R.R., Xie, S.D., 2023c. Variations of Wintertime Ambient Volatile Organic Compounds in Beijing, China, from 2015 to 2019. Environ. Sci. Technol. Lett. 10, 131–136.
Li, J., Wu, R., Li, Y., Hao, Y., Xie, S., Zeng, L., 2016b. Effects of rigorous emission controls on reducing ambient volatile organic compounds in Beijing, China. Sci. Total Environ. 557, 531–541.
Li, J.Y., Zhang, H.W., Li, L., Ye, F., Wang, H.L., Guo, S., Zhang, N., Qin, M.M., Hu, J.L., 2023b. Modeling secondary organic aerosols in China: state of the art and perspectives. Curr. Pollut. Rep. 9, 22–45.
Li, K., Li, J.L., Wang, W.G., Tong, S.R., Liggio, J., Ge, M.F., 2017. Evaluating the effectiveness of joint emission control policies on the reduction of ambient VOCs: implications from observation during the 2014 APEC summit in suburban Beijing. Atmos. Environ. 164, 117–127.
Li, Y., Lei, L., Sun, J.X., Gao, Y.Q., Wang, P., Wang, S.Y., Zhang, Z.L., Du, A.D., Li, Z.J., Wang, Z.F., Kim, J.Y., Kim, H., Zhang, H.L., Sun, Y.L., 2023a. Significant reductions in secondary aerosols after the three-year action plan in Beijing summer. Environ. Sci. Technol. 57, 15945–15955.
Li, Y., Poeschl, U., Shiraiwa, M., 2016c. Molecular corridors and parameterizations of volatility in the chemical evolution of organic aerosols. Atmos. Chem. Phys. 16, 3327–3344.
Li, Y., Zhou, W., Sun, J.X., Lei, L., Xu, W.Q., Zhang, Z.J., Zhang, Y., Du, A.D., Ye, P.L., Wang, J.F., Eleonora, A., Wang, Z.F., Douglas, R. Worsnop, Sun, Y.L., 2025. Oxygenated organic molecules in urban Beijing: contrasting summer–winter composition, sources, and roles in secondary organic aerosol Formation. Environ. Sci. Technol. 60, 4990–5004.
Lin, J.T., Liu, M.Y., Xin, J.Y., Boersma, K.F., Spurr, R., Martin, R., Zhang, Q., 2015. Influence of aerosols and surface reflectance on satellite NO_2 retrieval: seasonal and spatial characteristics and implications for NO_x emission constraints. Atmos. Chem. Phys. 15, 11217–11241.
Lin, J.T., Martin, R.V., Boersma, K.F., Sneep, M., Stammes, P., Spurr, R., Wang, P., Van Roozendael, M., Clémer, K., Irie, H., 2014. Retrieving tropospheric nitrogen dioxide from the Ozone Monitoring Instrument: effects of aerosols, surface reflectance anisotropy, and vertical profile of nitrogen dioxide. Atmos. Chem. Phys. 14, 1441–1461.
Liu, J., Chu, B., Chen, T., Zhong, C., Liu, C., Ma, Q., Ma, J., Zhang, P., He, H., 2021. Secondary organic aerosol Formation potential from ambient air in Beijing: effects of atmospheric oxidation capacity at different pollution levels. Environ. Sci. Technol. 55, 4565–4572.
Liu, L., Long, X., Li, Y., Zang, Z.L., Wang, F.W., Han, Y., Bao, Z.R., Chen, Y., Feng, T., Yang, J.X., 2025. Impacts of meteorology and emission reductions on haze pollution during the lockdown in the North China Plain. Atmos. Chem. Phys. 25, 1569–1585.
Liu, M.Y., Lin, J.T., Boersma, K.F., Pinardi, G., Wang, Y., Chimot, J., Wagner, T., Xie, P. H., Eskes, H., Van Roozendael, M., Hendrick, F., Wang, P.C., Wang, T., Yan, Y.Y., Chen, L.L., Ni, R.J., 2019. Improved aerosol correction for OMI tropospheric NO_2 retrieval over East Asia: constraint from CALIOP aerosol vertical profile. Atmos. Meas. Tech. 12, 1–21.
Liu, M.Y., Lin, J.T., Kong, H., Boersma, K.F., Eskes, H., Kanaya, Y., He, Q., Tian, X., Qin, K., Xie, P.H., Spurr, R., Ni, R.J., Yan, Y.Y., Weng, H.J., Wang, J.X., 2020. A new TROPOMI product for tropospheric NO_2 columns over East Asia with explicit aerosol corrections. Atmos. Meas. Tech. 13, 4247–4259.
Liu, Y., Xu, X.J., Yang, X.Y., He, J., Ji, D.S., Wang, Y.S., 2022. Significant reduction in fine particulate matter in Beijing during 2022 Beijing Winter olympics. Environ. Sci. Technol. Lett. 9, 822–828.
Liu, Y.F., Yin, S.J., Zhang, S.Q., Ma, W., Zhang, X., Qiu, P.P., Li, C.L., Wang, G.P., Hou, D. L., Zhang, X., An, J.L., Sun, Y.L., Li, J., Zhang, Z.Y., Chen, J., Tian, H.Z., Liu, X.A., Liu, L.Y., 2024. Drivers and impacts of decreasing concentrations of atmospheric volatile organic compounds (VOCs) in Beijing during 2016-2020. Sci. Total Environ. 906, 167847.
Mochida, M., Kawabata, A., Kawamura, K., Hatsushika, H., Yamazaki, K., 2003. Seasonal variation and origins of dicarboxylic acids in the marine atmosphere over the western North Pacific. J. Geophys. Res. Atmos. 108, 4193.
Molteni, U., Bianchi, F., Klein, F., El Haddad, I., Frege, C., Rossi, M.J., Dommen, J., Baltensperger, U., 2018. Formation of highly oxygenated organic molecules from aromatic compounds. Atmos. Chem. Phys. 18, 1909–1921.
Nguyen, T.B., Roach, P.J., Laskin, J., Laskin, A., Nizkorodov, S.A., 2011. Effect of humidity on the composition of isoprene photooxidation secondary organic aerosol. Atmos. Chem. Phys. 11, 6931–6944.
Nie, W., Yan, C., Huang, D.D., Wang, Z., Liu, Y.L., Qiao, X.H., Guo, Y.S., Tian, L.H., Zheng, P.G., Xu, Z.N., Li, Y.Y., Xu, Z., Qi, X.M., Sun, P., Wang, J.P., Zheng, F.X., Li, X. X., Yin, R.J., Dallenbach, K.R., Bianchi, F., Petäjä, T., Zhang, Y.J., Wang, M.Y., Schervish, M., Wang, S.N., Qiao, L.P., Wang, Q., Zhou, M., Wang, H.L., Yu, C., Yao, D.W., Guo, H., Ye, P.L., Lee, S.C., Li, Y.J., Liu, Y.C., Chi, X.G., Kerminen, V.-M., Ehn, M., Donahue, N.M., Wang, T., Huang, C., Kulmala, M., Worsnop, D., Jiang, J.K., Ding, A.J., 2022. Secondary organic aerosol formed by condensing anthropogenic vapours over China's megacities. Nat. Geosci. 15, 255–261.
Paatero, P., Tapper, U., 1994. Positive matrix factorization - a nonnegative factor model with optimal utilization of error-estimates of data values. Environmetrics 5, 111–126.
Petit, J.E., Favez, O., Sciare, J., Canonaco, F., Croteau, P., Močnik, G., Jayne, J., Worsnop, D., Leoz-Garziandia, E., 2014. Submicron aerosol source apportionment of wintertime pollution in Paris, France by double positive matrix factorization (PMF2) using an aerosol chemical speciation monitor (ACSM) and a multi-wavelength aethalometer. Atmos. Chem. Phys. 14, 13773–13787.
Price, D.J., Day, D.A., Pagonis, D., Stark, H., Handschy, A.V., Algrim, L.B., Miller, S.L., de Gouw, J.A., Ziemann, P.J., Jimenez, J.L., 2021. Sources of gas-phase species in an art Museum from comprehensive real-time measurements. ACS Earth Space Chem. 5, 2252–2267.
Qu, Q., Wang, S., Zhao, B., Hu, R., Liang, C., Zhang, H., Li, S., Feng, B., Hou, X., Yin, D., Du, J., Chu, Y., Zhang, Y., Wu, Q., Wen, Y., Wu, X., Hu, J., Zhang, S., Hao, J., 2024. Response of organic aerosol in Beijing to emission reductions during the XXIV Olympic Winter Games. Sci. Total Environ. 914, 170033.
Ren, Y.C., Wang, G.Q., Zhang, Q.Z., Tao, C.L., Ji, S.P., Wang, Q., Wang, W.X., 2025. The impact of Chinese new year on air quality in north China based on machine learning. Atmos. Environ. 342, 120874.
Reyes-Villegas, E., Bannan, T., Le Breton, M., Mehra, A., Priestley, M., Percival, C., Coe, H., Allan, J.D., 2018. Online chemical characterization of food-cooking organic aerosols: implications for source apportionment. Environ. Sci. Technol. 52, 5308–5318.
Riva, M., Rantala, P., Krechmer, J.E., Peräkylä, O., Zhang, Y., Heikkinen, L., Garmash, O., Yan, C., Kulmala, M., Worsnop, D., Ehn, M., 2019. Evaluating the performance of five different chemical ionization techniques for detecting gaseous oxygenated organic species. Atmos. Meas. Tech. 12, 2403–2421.
Saha, P.K., Reece, S.M., Grieshop, A.P., 2018. Seasonally varying secondary organic aerosol Formation from In-Situ oxidation of near-highway air. Environ. Sci. Technol. 52, 7192–7202.
Shen, X., Che, H., Lv, T., Wu, B., Cao, X., Li, X., Zhang, H., Hao, X., Zhou, Q., Yao, Z., 2023. Real-world emission characteristics of semivolatile/intermediate-volatility organic compounds originating from nonroad construction machinery in the working process. Sci. Total Environ. 858, 159970.
Sun, Y.L., He, Y., Kuang, Y., Xu, W.Y., Song, S.J., Ma, N., Tao, J.C., Cheng, P., Wu, C., Su, H., Cheng, Y.F., Xie, C.H., Chen, C., Lei, L., Qiu, Y.M., Fu, P.Q., Croteau, P., Worsnop, D.R., 2020b. Chemical differences between PM_1 and $PM_{2.5}$ in highly polluted environment and implications in air pollution studies. Geophys. Res. Lett. 47 e2019GL086288.
Sun, Y.L., Lei, L., Zhou, W., Chen, C., He, Y., Sun, J.X., Li, Z.J., Xu, W.Q., Wang, Q.Q., Ji, D.S., Fu, P.Q., Wang, Z.F., Worsnop, D.R., 2020a. A chemical cocktail during the COVID-19 outbreak in Beijing, China: insights from six-year aerosol particle composition measurements during the Chinese New Year holiday. Sci. Total Environ. 742, 140739.
Sun, Y.L., Luo, H., Li, Y., Zhou, W., Xu, W.Q., Fu, P.Q., Zhao, D.F., 2025. Atmospheric organic aerosols: online molecular characterization and environmental impacts. npj Clim. Atmos. Sci. 8, 305.
Sun, Y.L., Wang, Z.F., Wild, O., Xu, W.Q., Chen, C., Fu, P.Q., Du, W., Zhou, L.B., Zhang, Q., Han, T.T., Wang, Q.Q., Pan, X.L., Zheng, H.T., Li, J., Guo, X.F., Liu, J.G., Worsnop, D.R., 2016. "APEC Blue": secondary aerosol reductions from emission controls in Beijing. Sci. Rep. 6, 20668.
Tao, W.W., Primbs, T., Shu, T., Simonich, S.L.M., 2009. Atmospheric particulate matter pollution during the 2008 Beijing olympics. Environ. Sci. Technol. 43, 6440.
Ulbrich, I.M., Canagaratna, M.R., Zhang, Q., Worsnop, D.R., Jimenez, J.L., 2009. Interpretation of organic components from Positive Matrix Factorization of aerosol mass spectrometric data. Atmos. Chem. Phys. 9, 2891–2918.
Wang, Y.H., Liu, Z.R., Zhang, J.K., Hu, B., Ji, D.S., Yu, Y.C., Wang, Y.S., 2015. Aerosol physicochemical properties and implications for visibility during an intense haze episode during winter in Beijing. Atmos. Chem. Phys. 15, 3205–3215.
Wu, R., Vereecken, L., Tsiligiannis, E., Kang, S., Albrecht, S.R., Hantschke, L., Zhao, D., Novelli, A., Fuchs, H., Tillmann, R., Hohaus, T., Carlsson, P.T.M., Shenolikar, J., Bernard, F., Crowley, J.N., Fry, J.L., Brownwood, B., Thornton, J.A., Brown, S.S., Kiendler-Scharr, A., Wahner, A., Hallquist, M., Mentel, T.F., 2021. Molecular composition and volatility of multi-generation products formed from isoprene oxidation by nitrate radical. Atmos. Chem. Phys. 21, 10799–10824.
Xu, W., Chen, C., Qiu, Y.M., Xie, C.H., Chen, Y.L., Ma, N., Xu, W.Y., Fu, P.Q., Wang, Z.F., Pan, X.L., Zhu, J., Nga, Lee Ngcgh, Sun, Y.L., 2021. Size-resolved characterization of organic aerosol in the North China Plain: new insights from high resolution spectral analysis. Environ. Sci. Atmos. 1, 346–358.

Xu, W.Q., Li, Z.J., Lambe, A.T., Li, J., Liu, T., Du, A.D., Zhang, Z.Q., Zhou, W., Sun, Y.L., 2022. Secondary organic aerosol formation and aging from ambient air in an oxidation flow reactor during wintertime in Beijing, China. Environ. Res. 209, 112751.

Xu, W.Q., Sun, Y.L., Chen, C., Du, W., Han, T.T., Wang, Q.Q., Fu, P.Q., Wang, Z.F., Zhao, X.J., Zhou, L.B., Ji, D.S., Wang, P.C., Worsnop, D.R., 2015. Aerosol composition, oxidation properties, and sources in Beijing: results from the 2014 Asia-Pacific Economic Cooperation summit study. Atmos. Chem. Phys. 15, 13681–13698.

Yang, G., Wei, W., Lv, Z.F., Cheng, S.Y., Li, Y., 2016. Characteristics of VOCs in Beijing urban area during APEC period and its verification for VOCs emission inventory. China Environ. Sci. 36, 1297–1304.

Ye, C.S., Yuan, B., Lin, Y., Wang, Z.L., Hu, W.W., Li, T.G., Chen, W., Wu, C.H., Wang, C. M., Huang, S., Qi, J.P., Wang, B.L., Wang, C., Song, W., Wang, X.M., Zheng, E., Krechmer, J.E., Ye, P.L., Zhang, Z.Y., Wang, X.M., Worsnop, D.R., Shao, M., 2021. Chemical characterization of oxygenated organic compounds in the gas phase and particle phase using iodide CIMS with FIGAERO in urban air. Atmos. Chem. Phys. 21, 8455–8478.

Zhang, Y., Tang, L., Croteau, P.L., Favez, O., Sun, Y., Canagaratna, M.R., Wang, Z., Couvidat, F., Albinet, A., Zhang, H., Sciare, J., Prevot, A.S.H., Jayne, J.T., Worsnop, D.R., 2017. Field characterization of the $PM_{2.5}$ Aerosol Chemical Speciation Monitor: insights into the composition, sources, and processes of fine particles in eastern China. Atmos. Chem. Phys. 17, 14501–14517.

Zhang, Y.J., Tang, L.L., Wang, Z., Yu, H.X., Sun, Y.L., Liu, D., Qin, W., Canonaco, F., Prevot, A.S.H., Zhang, H.L., Zhou, H.C., 2015. Insights into characteristics, sources, and evolution of submicron aerosols during harvest seasons in the Yangtze River delta region, China. Atmos. Chem. Phys. 15, 1331–1349.

Zhang, Z.J., Xu, W.Q., Zeng, S.Q., Liu, Y.C., Liu, T.Y., Zhang, Y., Du, A.D., Li, Y., Zhang, N., Wang, J.F., Aruffo, E., Han, P.F., Li, J., Wang, Z.F., Sun, Y.L., 2024. Secondary organic aerosol Formation from ambient air in summer in urban Beijing: contribution of S/IVOCs and impacts of heat waves. Environ. Sci. Technol. Lett. 11, 738–745.

Zhao, J., Du, W., Zhang, Y.J., Wang, Q.Q., Chen, C., Xu, W.Q., Han, T.T., Wang, Y.Y., Fu, P.Q., Wang, Z.F., Li, Z.Q., Sun, Y.L., 2017. Insights into aerosol chemistry during the 2015 China Victory Day parade: results from simultaneous measurements at ground level and 260 m in Beijing. Atmos. Chem. Phys. 17, 3215–3232.

Zheng, H.T., Chang, X., Wang, S.X., Li, S.Y., Yin, D.J., Zhao, B., Huang, G.H., Huang, L., Jiang, Y.Q., Dong, Z.X., He, Y.C., Huang, C., Xing, J., 2023a. Trends of Full-Volatility Organic Emissions in China from 2005 to 2019 and their Organic Aerosol Formation Potentials. Environ. Sci. Technol. Lett. 10, 137–144.

Zheng, P., Chen, Y., Wang, Z., Liu, Y., Pu, W., Yu, C., Xia, M., Xu, Y., Guo, J., Guo, Y., Tian, L., Qiao, X., Huang, D.D., Yan, C., Nie, W., Worsnop, D.R., Lee, S., Wang, T., 2023b. Molecular characterization of oxygenated organic molecules and their dominating roles in particle growth in Hong Kong. Environ. Sci. Technol. 57, 7764–7776.

Zheng, Y., Cheng, X., Liao, K., Li, Y., Li, Y., Hu, W., Liu, Y., Zhu, T., Chen, S., Zeng, L., Worsnop, D., Chen, Q., Huang, R.-J., 2020. Characterization of anthropogenic organic aerosols by TOF-ACSM with the new capture vaporizer. Atmos. Meas. Tech. 13, 2457–2472.

Zhou, W., Lei, L., Du, A.D., Zhang, Z.Q., Li, Y., Yang, Y., Tang, G.Q., Chen, C., Xu, W.Q., Sun, J.X., Li, Z.J., Fu, P.Q., Wang, Z.F., Sun, Y.L., 2022. Unexpected increases of severe haze pollution during the post COVID-19 period: effects of emissions, meteorology, and secondary production. J. Geophys. Res. Atmos. 127 e2021JD035710.

Zhou, W., Xu, W.Q., Li, Z.J., Lei, L., Li, Y., Sun, J.X., Du, A.D., Zhang, Z.Q., Li, Y., Fu, P. Q., Ge, X.L., Sun, Y.L., 2024. Molecular characterization of gaseous organic acids and nitrogen-containing compounds from crop straw and wood burning. J. Geophys. Res. Atmos. 129 e2023JD040568.